frontiers

Isometric Torque Values About Robotic Knee Using Braided Pneumatic Actuators

Ben Bolen [1,*], **Lindie Burgess** [1], **Connor Morrow** [1], **Aidan Vogt** [1], **Cody Scharzenberger** [1], **Lawrence Pang** [1], **and Alex Hunt** [1]

[1] *Agile and Adaptive Robotics Laboratory, Portland State University, Department of Mechanical and Materials Engineering, Portland, OR, USA*

Correspondence*:
Ben Bolen, Portland State University, Department of Mechanical and Materials Engineering, 1930 SW 4th Ave., Portland, OR, 97207, USA
bbolen83@gmail.com

ABSTRACT

A lower limb model of a bipedal humanoid robot was designed to achieve biomimetic ranges of motion and isometric torque values. An important component of this robot is a biomimetic four-bar linkage knee joint that allows the joint to have two degrees of freedom (DoF) over a range of knee flexion and extension values. This joint is actuated with artificial muscles called braided pneumatic actuators (BPAs). While these artificial muscles have force-length curves that are grossly similar to real muscles, they have other limitations that need to be considered, such as their lower maximum contractile capacity and flexibility when compared to human muscles. An isometric robot knee torque test stand was created to determine several things. The first task was to quantify results for actuators of different initial length and configuration. Second, use that data to characterize the difference between theoretical calculations and actual results so that we may modify the theoretical calculations. To do this, we simplified the muscle arrangement on the robotic leg so that it consists of a pair of antagonistic uniarticular flexor/extensor muscles. Another robot knee was designed using similar muscle origin insertion locations but this knee was used a simpler 1-DoF revolute joint. Testing for isometric knee torque values in these configurations allowed for the quantification of difference between measured and expected results, as well as a quantification of the factors that were important in these differences.

Keywords: BPA, Biomimetic, Function Fit, PAM, Artificial Muscle, Bioinspired, Bipedal Robot, Isometric Knee Torque

1 INTRODUCTION

Both academic researchers and the general public are keenly interested in biomimetic humanoid robots due to their many applications. In the discipline of biomimetic robotics, high fidelity humanoid robots can help improve our understanding of both human biomechanics and the underlying neuromechanical systems that control them (Shin et al., 2018; Asano et al., 2019). Experiments can be done with robots that would not be practical nor ethical if done on human test subjects, and modifying robotic platforms is a potentially faster and cheaper alternative to human observation studies.

For truly biomimetic humanoid robots to go a step beyond being merely bio-inspired, it is unclear how the actuator affects other aspects of the control. One requirement for proposed artificial muscle-actuators should be that they be able to produce isometric torque about humanoid joints that meets or exceeds values

measured in humans. There are several interesting methods of actuating robotic joints, including artificial muscles, electric motors (either directly driving the joints **(citations?)**or via cable systems **(citations?)**) , or hydraulics. Electric motors tend to required a lot of power, generate a lot of heat, and have torque curves unlike that of real muscles. Hydraulic actuators are heavy and require a dedicated hydraulic fluid system to operate. Electrically stimulated artificial muscles are new and do not yet produce very much force. McKibben style braided pneumatic actuators (BPAs, also called Pneumatic Artificial Muscles or PAMs) are a promising method of actuation because they have low weight, high force/weight ratio, and a force-length curve that is grossly similar to actual muscle. Routing these muscles in a biomimetic arrangement can allow us to investigate and mimic the torque produced about joints by actual human muscle.

Previous robots that use artificial muscles do not show significant design considerations for the forces and torques that the muscles will produce. However, these aspects are critical for further understanding how muscles are controlled (**citation?**) in animals. As a consequence of this, these robots typically do not faithfully attempt to replicate the number of existing muscle actuators. They also tend to use a single degree of freedom (DoF) knee joints, while knees are actually better modeled as 2-DoF sliding and rotating joints. They instead focus on planar, uniarticular muscle arrangements. Our research diverges from these robots by attempting to correct for these deficiencies.

Our previous research has laid the groundwork to start building a bipedal robot with biomimetic humanoid joints and artificial muscle actuator paths. Investigating the isometric force profile of 10 mm Festo Braided Pneumatic Actuators (BPAs, also called Pneumatic Artificial Muscle or PAMs) demonstrated artificial muscles that can be made to have a similar isometric force profile to human muscle (Hunt et al., 2017). Research on a humanoid artificial knee allowed us to build a biomimetic translating sliding knee joint (Steele et al., 2017) instead of the traditional pinned robotic joint. A more recent paper on artificial muscle attachment locations for a humanoid robot produced theoretical isometric torque curves (Bolen and Hunt, 2019). Optimization of these muscle paths and attachment locations was done by Morrow to produce a torque curve and muscle path that match the robotic system more closely to the human biomechanical benchmark we are using (Morrow et al., 2020). All of the concepts can be combined to build an artificial human leg and test the validity of our theory.

These previous studies need to be combined and tested on a physical robot body. The 10 mm inner diameter (ID) Festo BPAs have been characterized (Hunt et al., 2017), but the $20\,\mathrm{mm}$ and $40\,\mathrm{mm}$ ID BPAs have not been. In our previous work (Bolen and Hunt, 2019; Morrow et al., 2020), moment arms have been calculated by the unit vector cross product method presented show in Hoy (Hoy et al., 1990), but not the change in muscle length over change in angle method that Hoy and others (Hoy et al., 1990; Yamaguchi and Zajac, 1989; Sherman et al., 2013; Delp et al., 1990; Seth et al., 2011) have also used. It is not known if one method is more correct than the other. Knee Instantaneous Center of Rotation (ICR) differs between the Steele model (Steele et al., 2018) and the OpenSim model Delp et al. (1990); Seth et al. (2018) model. This fact, as well as changes in the knee geometry and muscle placement, means there will be different muscle moment arms between the models. The differences in isometric torque between the theoretical, measured, and human biomechanical benchmark model need to be investigated.

Deviation from expected versus measured force in BPAs can happen in several ways. Festo reports that there can be a 10% deviation from theoretical force ((Corporation, 2022)). Joint friction can cause a decrease in torque, as can non-rigid elements of the artificial leg and test frame. Kinking of the artificial muscle as it wraps around a joint also is predicted to reduce the amount of available force. A further reduction in force, and therefore torque, can be expected from a previously undefined reduction in force that happens as BPAs resting length is decreased.

We hypothesize that the isometric torque values that we measure experimentally will be lower than what is predicted by our theoretical model. A correction factor can then be applied to our calculations which will improve our results. The modified design tools we previously developed can be compared to measured isometric torque values produced by our artificial muscles about the robot knee joint, which will then be used to update how we design and analyze biomimetic joints in the future (including determining which, if any, method of calculating moment arm is the best). Future designs can then be built with artificial muscles that meet or exceed human isometric torque values.

2 METHODS AND MATERIALS

An important initial step for biomimetic humanoid robot research is to see if these robots, actuated by artificial muscles, can meet or exceed isometric torque values that are produced by human muscles (or groups of muscle actuators, in some cases). Previous research has demonstrated meeting or exceeding these human values with BPAs is at least theoretically plausible (Bolen and Hunt, 2019; Morrow et al., 2020), so the next logical step is to test this on an actual robot. To accomplish this, we built a test jig to run these experiments. With the expectation that measured results will be less than theoretical, it was also necessary to simplify the robot muscle arrangement and knee design to elucidate the variables that affect the results. There are, therefore, three models that we must consider, including: (1) the human biomechanical model, (2) the conceptual robot model, and (3) the actual robot model. Within the conceptual and actual robot models, we varied the knee actuation by using either a simplified pinned knee joint or a biomimetic 2-DoF knee, and muscles to either flex or extend the joint. Furthermore we varied the artificial muscle origin/insertion locations, resting lengths, diameters, and whether or not they used an artificial tendon These results were compared to the baseline model.

After running these tests it was important to verify that the equation developed in (Hunt et al., 2017) was applicable to longer resting BPA lengths and forces in (Bolen and Hunt, 2019; Morrow et al., 2020). Comparing the discrepancy in force values expected from this equation to values we determined experimentally with additional BPA lengths, it was necessary to derive additional equations to characterize the Festo BPAs. During this process, we found an equation for maximum force in the $10\,\mathrm{mm}$ BPA as a function of resting length, a normalized equation for force as a function of relative strain and relative pressure, and were unable to find a relationship between maximum contraction and resting length.

2.1 Robot Architecture

The biomimetic robot leg assembly is for a two legged robot with 2-DoF knee joint first introduced in (Steele et al., 2017). The 2-DoFs are achieved by using a four bar linkage mechanism. The leg assembly is based off of bones scans of someone 6 ft tall (approx. 1.83 m) and the OpenSim Gait2392 model. Each joint is driven by two antagonistic Festo actuators which act as artificial muscles. A test jig constrains the robot to saggital planar motion 1. This system has two mounting locations to fix the femur to the frame. To eliminate the effect of gravity on our test results the robot saggital plane was made parallel with the horizontal plane of the ground. This enables longitudinal, vertical, and pitch movements (e.g. knee joint flexion/extension). while constraining lateral, roll, and yaw DoFs.

The actuators are Festo brand BPAs of inner diameter (ID) $10\,\mathrm{mm}$, $20\,\mathrm{mm}$ and $40\,\mathrm{mm}$ size. Each actuator is connected in series with a Freescale MPX5700 GP gauge pressure sensor. Joint and load cell angles are collected with digital or analog goniometers. Analog data from the pressure sensor is converted to digital data with a microcontroller, which then passes that data on to a Windows 10 PC or a Windows 11 laptop. Force is measured by reading the screen of a crane scale or using a load cell. When using a load

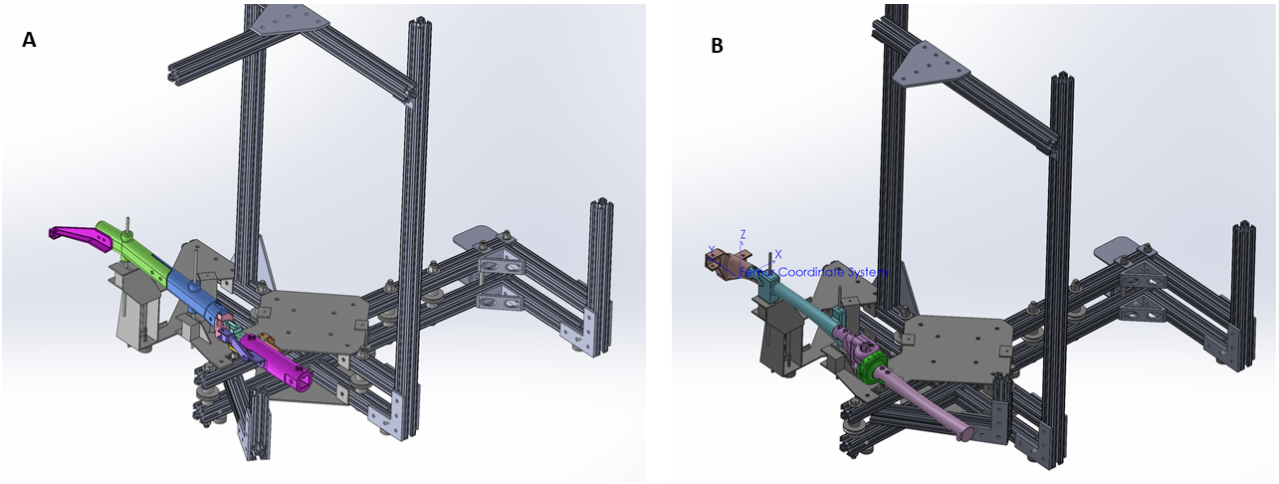

Figure 1. Solid model assemblies of two different robotic legs in the test stand using either **(A)** a revolute joint knee, or **(B)** a biomimetic knee.

cell the data is passed to a HX711 24-bit analog-to-digital converter (ADC), and then the microcontroller to computer connection previously mentioned.

Components of the robot leg are the knee joint, femur, tibia, BPAs, BPA end caps, artificial tendon (where noted), and attachment brackets 2. The artificial bone components are 3D printed using Onyx material on Markforged Onyx One and Mark Two printers. Onyx is a proprietary Markforged material that consists of chopped carbon fiber in nylon. Certain brackets also included carbon fiber layers to increase stiffness. Artificial tendon is made with Shimano bicycle brake cable for $\phi 10\,\mathrm{mm}$ BPAs, and wire rope with the $20\,\mathrm{mm}$ and $40\,\mathrm{mm}$ ID BPAs. When using the brake cable we first apply load to it and induce plastic deformation so that during the test the cable only has elastic deformation.

In many cases, the goal is to determine the maximum isometric torque a BPA can produce in a given configuration. Therefore the BPAs to must be inflated full pressure (which we defined as the somewhat-standard building air supply pressure of $620\,\mathrm{kPa}$). We chose to use one uniarticular knee extensor and one uniarticular knee flexor. The revolute joint knee tests used 10 mm Festo BPAs only. The Biceps Femoris Short Head muscle was mimicked using a 20 mm Festo BPA. The human vastus intermedius, vastus lateralis, and vastus medialis are mimicked using one over-strength robotic vastus intermedius BPA of 40 mm internal diamter (ID). We designed our own end caps for the actuators and printed them in Onyx. One of the cap styles is designed to be pinned to the muscle origin location, while the other style of end cap style is free floating and attaches to the muscle insertion location via an artificial tendon. During tests where both ends were pinned, only the former style of end cap was used.

Larger diameter BPA lengths for the humanoid knee were determined using the optimization procedure described by (Morrow et al., 2020). Actuator origin and insertion attachment points locations are in the femoral and tibial reference frames. These reference frames are discussed in the next section.

2.1.1 Robotic Knee Joints

We used the sliding contact knee that was designed by Steele (Steele et al., 2018, 2017). The knee is sliding contact and was designed to reduce wear. In practice, not much contact occured between the condylar surface and the tibial head. This design uses a four bar linkage that allows the joint origin to translate in the $\hat{y}$ and $\hat{y}$ directions during knee rotation 3. Typically, a reference is located at the joint center.

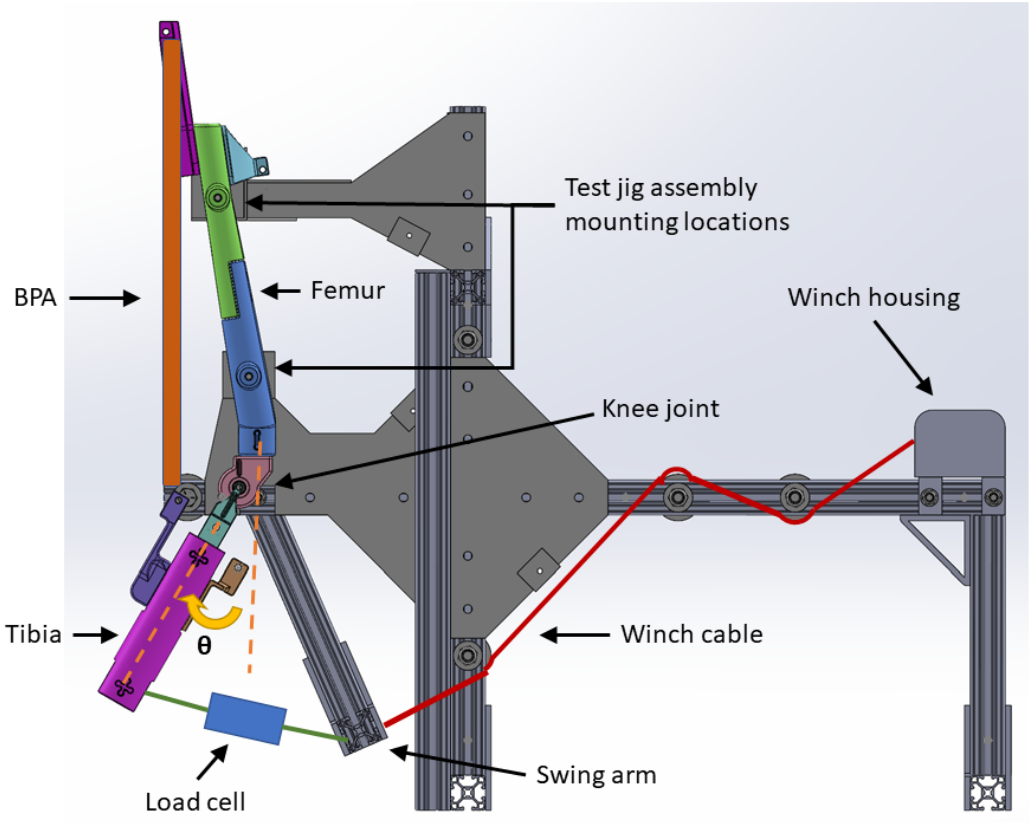

Figure 2. 1-DoF pinned-joint robot knee in the test apparatus with important components labeled. Leg is shown with 30 degrees flexion, i.e. $\theta_k = -30°$

The linkage has an Instantaneous Center of Rotation (ICR) at the intersection of the links. To more directly compare our results with the OpenSim model, and in the interest of simplifying our model's transformation matrices, we arbitrarily defined a joint location that moved in a similar way to the human biomechanical model 3. Both models had the same home position location, as did the pinned knee joint.

The differences in the knee X and Y position as a function of knee angle are show in 4. The muscle origin and insertion locations for each configuration is listed in 1. With the reference frames and muscle path geometry defined, it is then possible to calculate torque values that the muscles can produce about the joint.

2.2 Moment arm and Torque calculations

Compare measured robot performance to robot calculations, but also to what we expected from a human's reported maximum isometric force. Given a point of interest and a force vector $\vec{F}$, there exists a distance $\vec{d}$ from the point of interest to the line of action represented by $\vec{F}$. The classical mechanics way to calculate torque $\vec{M}$ about the point of interest is to take the cross product of distance $\vec{d}$ and force vector $\vec{F}$ 1.

$$\vec{M} = \vec{d} \times \vec{F} \tag{1}$$

The calculations for human muscle force that we used as a benchmark were from Delp, Hoy, Yamaguchi, Sherman, Millard, and Thelen (Delp et al., 1990; Hoy et al., 1990; Yamaguchi and Zajac, 1989; Sherman et al., 2013; Millard et al., 2013; Thelen, 2003). Reference human values were obtained using the Gait2392

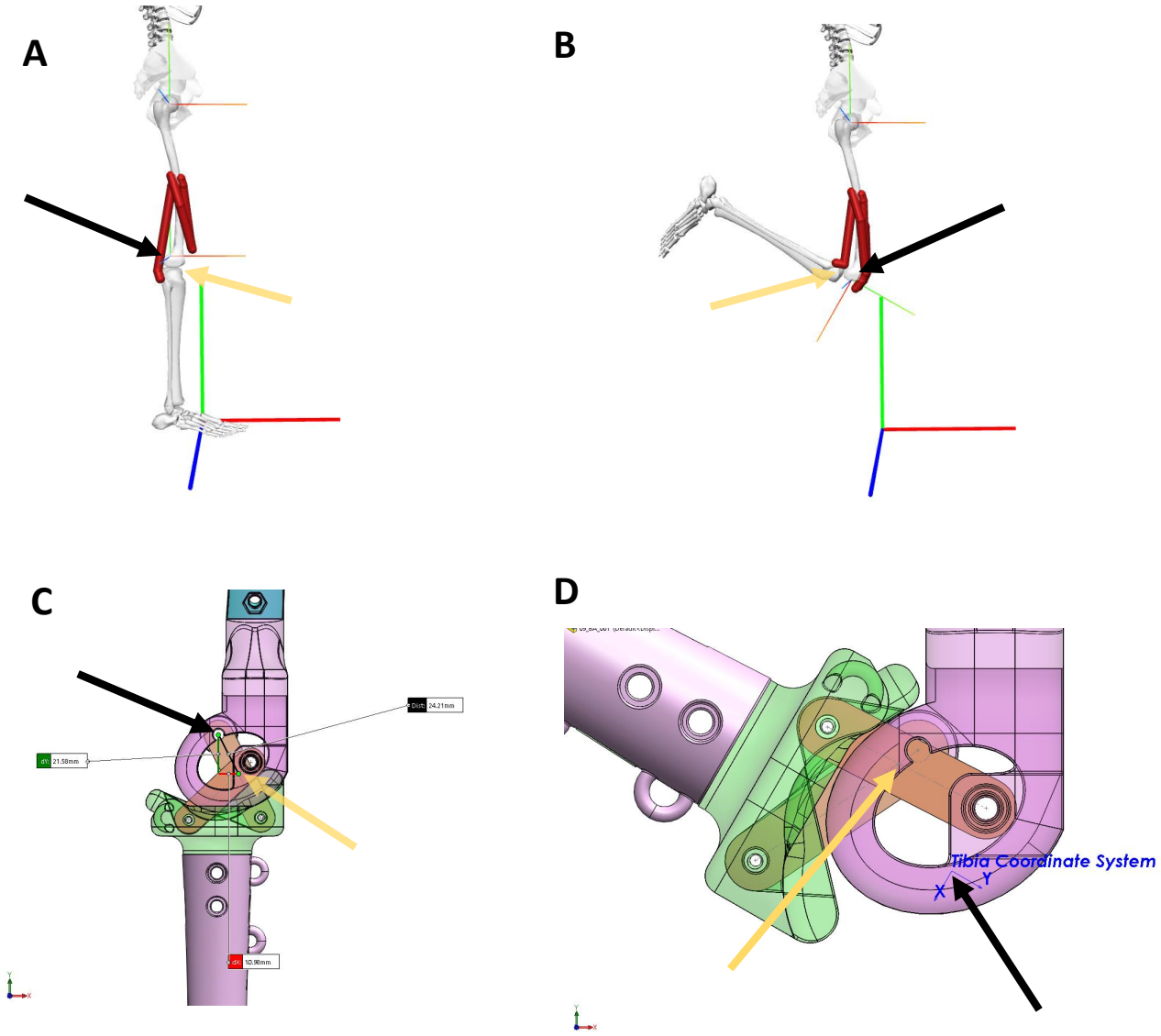

Figure 3. Refernce frames for Gait2392 in **(A)** home position and **(B)** flexed ($\theta = -120°$). Frames for biomimetic robot knee in **(C)** home position and **(D)** flexed ($\theta = -120°$). Coordinate directions are: $\hat{x}$ in red, $\hat{y}$ in green, and $\hat{z}$ in blue. Spatial frame is s and body frame is b. For **(A)** and **(B)**: black arrows point to the tibia reference frame as defined by OpenSim, yellow arrows point to the actual ICR (the tibial-femoral contact point), the large axes are general space frames, and the small axes represent body frames for the hip h and knee k. For **(C)** and **(D)**: black arrows point to the tibia reference frame as arbitrarily defined by us ($\vec{p}_k$ is at θ_3 (see (Steele et al., 2017) for details) when knee angle $\theta_k = 0$ and follows a similar path to the Gait2392 model), yellow arrows point to the actual ICR (intersection point of the two links).

model in the biomechanical modeling software OpenSim (Delp et al., 1990; Seth et al., 2011, 2018). Gait2392 is the anatomical human biomechanical model used for comparison 5. Moment arm r_θ is calculated by these sources using the following formula.

$$r_\theta = \frac{dl_m}{d\theta} \tag{2}$$

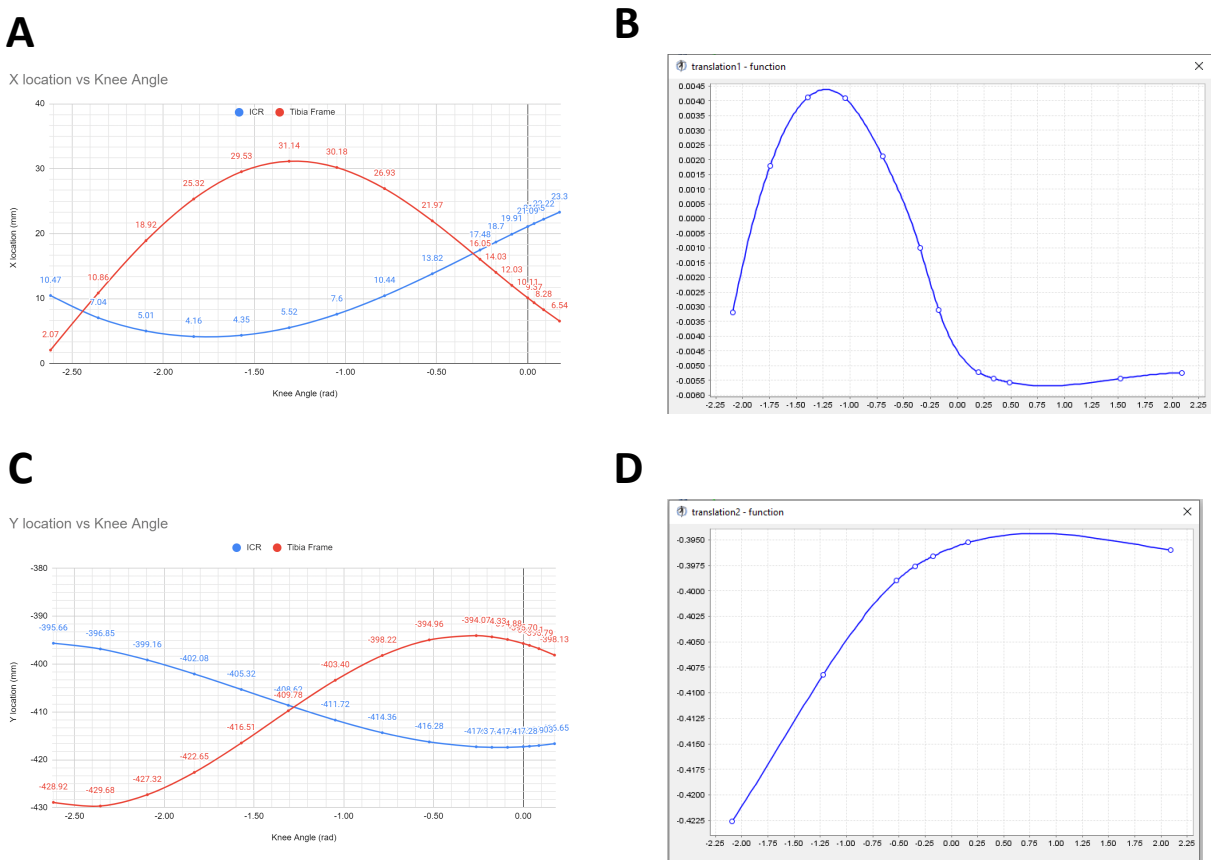

Figure 4. Comparison of joint X and Y positions (with respect to femur frame origin) as a function of knee angle. **(A)**: X axis location (in millimeters) for tibial frame (red) and ICR (blue) for the biomimetic knee as a function of knee angle (in radians). **(B)**: X axis location (in meters) for tibial frame as a function of knee angle (radians). **(C)**: Y axis location (in millimeters) for tibial frame (red) and ICR (blue) for the biomimetic knee as a function of knee angle (in radians). **(D)**: Y axis location (in meters) for tibial frame as a function of knee angle (radians).

where dl is the change in muscle length l_m and $d\theta$ is the change in joint angle. We opted out of using this method. Instead, we used the method developed by Young and colleagues (Young et al., 2019). The moment arm length for moments that produce torque about the $\hat{z}$ axis is $r_{\hat{k}}$.

$$r_{\hat{k}} = p_{\vec{proj},i} \cdot \frac{\vec{p_f} \times \hat{k}}{\|\vec{p_f} \times \hat{k}\|} \tag{3}$$

$p_{\vec{proj},i}$ is the free muscle segment projected onto the plane of interest defined by the joint axis. $\vec{p_f}$ is the projected muscle segment vector.

2.3 Data Collection: Equipment and Procedures

We built a test stand to take isometric knee torque measurements at different knee angles over its RoM. The test stand frame is made predominantly out of 80/20 components. The knee joint is allowed to rotate while the femur is fixed to the frame. A force sensor has one end connected to the tibia and the other is connected to a swing arm. The swing arm is tied to the winch with $3/16$ inch Kevlar rope from Quality™

Figure 5. View of the human biomechanical model Gait2392 used for comparison. In this test we looked at the uniarticular muscles that attach to the femur and cross the knee, shown as red muscle actuators in the picture.

Nylon Rope 3. This rope has a Kevlar core with a polyester jacket and is rated to have a break strength of 1150 lbs.

Force data was collected using one of two different sensors. The first was a MODERN STEP $300\,\mathrm{kg}$ digital crane scale. The second force sensor is a CALT DYLY-103 $100\,\mathrm{kg}$ S shaped load cell. The was load cell was used in conjunction with a HX711 Load Cell Amplifier. Pressure data came from a Freescale MPX5700 GP $5\,\mathrm{V}$ pressure sensor. Building air supply pressure was controlled with two pressure regulators in series.

The first is a Parker model 20R113GC 0-120 psi pressure regulator. The second is a Husky $3/8$ $in.$ High Performance Air Regulator HDA72200. A Festo VTUG-10-MRCR-S1T-26V20-T516LA-UL-T532S-8K valve manifold VTUG-G was used to deliver air from the pressure regulator to the actuator. This manifold is comprised of eight two-in-one bidirectional normally closed Festo VUVG-S10-T32C-AZT-M5-1T1L valves.

Pressure and load cell amplifier data are sent to Matlab via an Arduino Uno style Sparkfun BlackBoard C microcontroller. The computers that used Matlab were running Windows 10 and Windows 11. During phases when the Arduino was collecting force and pressure data to send to Matlab, the Arduino would also trigger (via Matlab) an onsemi 2N4401 NPN transistor to make valve manifold opened or close the valve. For other data collection the valve was manually opened and closed 7.

Length measurements were done using a FANUC tape measure. When measuring the knee extensor length, at times this was done by using a flexible piece of string to determine the axial length, then measuring that string with the tape measure. Other times we were able to measure the extensor length using iBayam flexible tape measures.

Angle measurements were taken with either a Medigauge digital electronic goniometer or with MALENOO analog goniometers of 6, 8, or 12 inch lengths. The angle of the knee joint and the angle of the force sensor to the moment arm were the measurements of interest to us. The latter angle allows us to calculate torque as the force sensor was not always perpendicular with the moment arm.

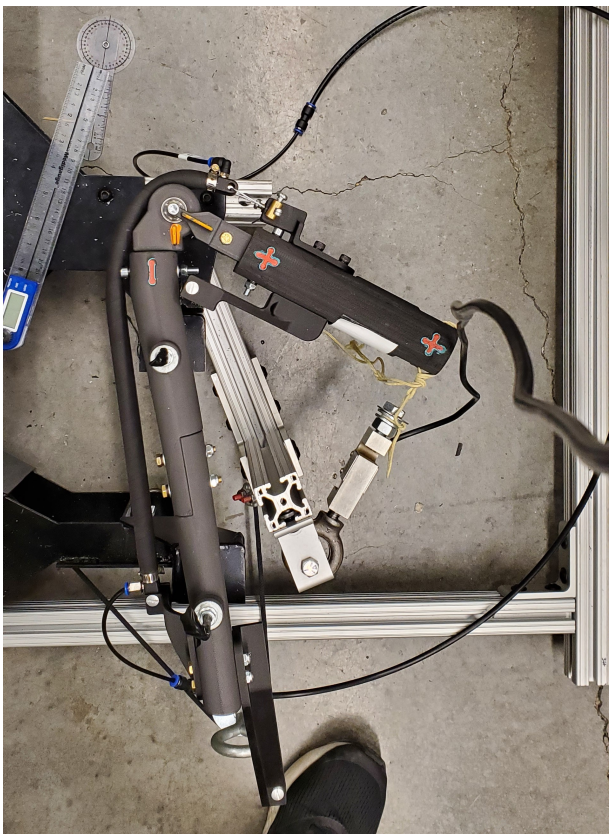

Figure 6. Robot leg in test jig. Setup shows the pinned knee configured for a test of the extensor BPA.The knee is positioned at $\theta_k = -120°$ flexion. The S shaped load cell attaches the tibia to the swing arm and is nearly perpendicular to the tibia in this configuration. Also note the compressed shape of the BPA during this high degree of flexion.

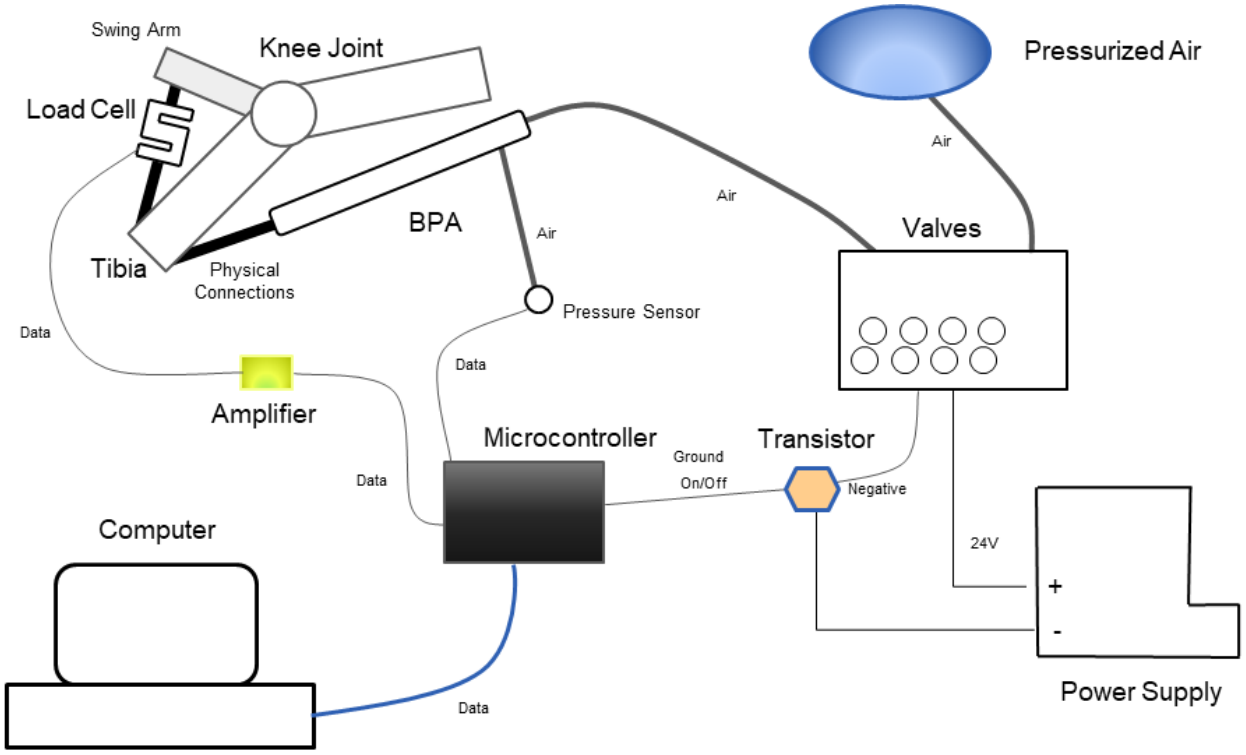

Figure 7. Data collection setup

2.4 Actuator Force Calculation

Human muscle-actuator force is calculated using the Hill muscle model. Specifically, we relied on the equations as described by Millard (Millard et al., 2013) and used in OpenSim model Gait 2392. The specifics equation and values are detailed in previous work by Bolen and Morrow (Bolen and Hunt, 2019; Morrow et al., 2020).

BPA actuator force in our previous work has been calculated from a length-tension-pressure relationship derived by Hunt (Hunt et al., 2017). For a given robot configuration and BPA pressure P (in kPa), the scalar force F (in Newtons) for each of the artificial muscles can be determined by solving the equation:

$$P = 254\,\text{kPa} + 1.23\,\frac{\text{kPa}}{\text{N}} \cdot F + 15.6\,\text{kPa} \cdot S + 192\,\text{kPa} \cdot \tan\left(2.03\left(\frac{\epsilon}{-0.331 \times 10^{-3}\,\frac{1}{\text{N}} \cdot F + \epsilon_{max}} - 0.46\right)\right) \quad (4)$$

ϵ is the amount of contraction, and ϵ_{max} is the maximum amount of contraction in a BPA without external load that is inflated to $620\,\text{kPa}$. S is the hysteresis factor of the artificial muscle in which $S = 1$ indicates the muscle is shortening and with $S = -1$ it is lengthening. For isometric contraction, set $S = 0$. An important note for (4) is that the coefficients have been updated with the correct values. We used this corrected version of the equation to create a lookup table for actuator force for a given amount of pressure and relative strain ϵ^*, defined as

$$\epsilon^* = \frac{\epsilon}{\epsilon_{max}} \tag{5}$$

With this lookup table created it is possible to use a curve fit to develop an equation for force as a function of pressure and relative strain. However, we note here two problems with the BPA characterization in (Hunt et al., 2017). The first is that this testing was done with a maximum of $111.2\,\mathrm{N}$ applied load, which is only about 20% of the maximum isometric force the Festo BPA is rated for at maximum pressure and no contraction. Secondly, we observed that maximum force in the BPAs decrease as the resting length decreases. Therefore, we created a test jig apparatus to test isometric force for various resting lengths of $10\,\mathrm{mm}$ Festo BPAs at different pressures.

Each BPA resting length, l_{rest}, is measured as the distance between the hose clamps. This is how Festo defines l_{rest}, although in (Hunt et al., 2017) it was measured to also include end cap length. We then inflated each BPA to maximum pressure ($P_{max} = 620\,\mathrm{kPa}$) and measured ϵ_{max}. The BPAs were then deflated, placed vertically in the test jig made out of 80/20 pieces and fixed between two crossmembers. The force sensor was placed between the upper crossmember and the BPA. For $120\,\mathrm{mm}$, $220\,\mathrm{mm}$, $260\,\mathrm{mm}$, $281\,\mathrm{mm}$ and $281\,\mathrm{mm}$ resting lengths, a Loadstar RAS1-01KS-S*C00 S Shaped load cell was used instead of the other force sensors previously mentioned. The distance between the crossmembers was adjusted to get different amounts of ϵ^*. The BPAs would then be inflated. BPAs with $120\,\mathrm{mm}$, $220\,\mathrm{mm}$, $260\,\mathrm{mm}$, $281\,\mathrm{mm}$ and $281\,\mathrm{mm}$ resting lengths had a lot of P variation, with only 4-5 different values of ϵ^* per BPA. Conversely, BPAs with resting lengths of $112\,\mathrm{mm}$, $415\,\mathrm{mm}$, $455\,\mathrm{mm}$, $490\,\mathrm{mm}$ and $518\,\mathrm{mm}$ had many different values of ϵ^* recorded, but all values were taken at or near P_{max}. Force and pressure data was collected as described in a previous section, above.

3 RESULTS

Results from BPA characterization tests are shown first in 8. Fig. 8**A** and 8**B** show a force response resembling an $\arctan$ curve along the resting length dimension and with a more linear response along the pressure axis. We used a surface fit to find the equation for maximum force in a $\phi 10\,\mathrm{mm}$ BPA as a function of resting length and pressure, i.e. $F_{max_{10}}(l_{rest}, P)$.

$$F_{max_{10}}(l_{rest}, P) = a1 \cdot P \cdot \arctan\left(a2 \cdot P \cdot (l_{rest} - 0.0075)\right) \tag{6}$$

l_{rest} is offset by $7.5\,\mathrm{mm}$ because solid modeling showed our end caps contact each other at this resting length. Therefore at this l_{rest} value no force could develop since air would flow in one endcap and out the other (assuming perfect alignment). The curve fitting was done using the Nonlinear Least Squares method and a Least Absolute Residual robustness. $a1 = 0.4848\,\mathrm{N\,kPa^{-1}}$ (0.4848–0.488 with 95% CI) and $a2 = 0.033\,06\,\mathrm{kPa^{-1}\,m^{-1}}$ (0.0325–0.03362 with 95% CI). 6 has an Adjusted $R^2 = 0.9997$ and an RMSE $= 2.749$. Substituting $P_{max} = 620\,\mathrm{kPa}$ into 6 yields the following simplified equation:

$$F_{max_{10}}(l_{rest}) = 301.6\,\mathrm{N} \cdot \arctan\left(20.5\,\mathrm{m^{-1}} \cdot (l_{rest} - 0.0075)\right) \tag{7}$$

Equation 7 is compared with the data in 8**B**. It can be seen that $\lim_{l_{rest}\to\infty} F_{max_{10}} = 473.7\,\mathrm{N}$. Fig. 8**C** shows an attempt at a linear fit for $\epsilon_{max}(l_{rest})$. There was a large amount of variance in the data, with the linear fit giving an adjusted $R^2 = 0.4124$ and an RMSE $= 0.0083$, therefore at this time we cannot say with confidence that there is a relationship between maximum strain and resting length.

The next step in BPA characterization we derived an equation for normalized force in the BPA, or $F^* = F/F_{max}$. In previous work we have already used relative strain $\epsilon^* = \epsilon/\epsilon_{max}$, and here we will also introduce relative pressure $P^* = P/P_{max}$. Then we can show that $F^*(\epsilon^*, P^*)$ 9. By visualizing the lookup tables discussed above, and the Festo Corporation data sheet, we can see that there appears to be an exponential relationship between ϵ^* and F, and a linear relationship between P and F. A polynomial surface fit also shows an interaction between the linear P and exponential ϵ^* terms. Therefore we fit a surface to the original data using an equation of the form

$$F^*(\epsilon^*, P) = b0 + \exp\left(-b1 \cdot \epsilon^*\right) + b2 + P\exp\left(-b3 \cdot (\epsilon^*)^2\right) + b4 + b5 \cdot P^* \tag{8}$$

With all the additional data collected on $10\,\mathrm{mm}$ ID BPAs with resting lengths given in 8, we then normalized the force data collected by dividing each BPA's force results by $F_{max_{10}}$ for that BPA. Pressure data was divided by P_{max} This reduced much of the variance in the data, as shown in Fig. 9, which qualitatively pointed towards using a surface fit as the right approach for F^*. Using ϵ^* and P^*, it was possible to reduce the amount of coefficients in Eq. 8 from six to only two. The equation for normalized force is

$$F^*(\epsilon^*, P^*) = -1 + \exp\left(-c1 \cdot \epsilon^*\right) + P^* \cdot \exp\left(-c2 \cdot (\epsilon^*)^2\right) \tag{9}$$

with $c1 = 1.7$ (1.692–1.708 with 95% CI) and $c2 = 0.2$ (0.1968–0.2029 with 95% CI). This surface fit was done using Nonlinear Least Squares method and Least Absolute Residuals robustness. Additional data from separate tests using the $120\,\mathrm{mm}$, $220\,\mathrm{mm}$, $260\,\mathrm{mm}$, $281\,\mathrm{mm}$ and $281\,\mathrm{mm}$ resting lengths were used

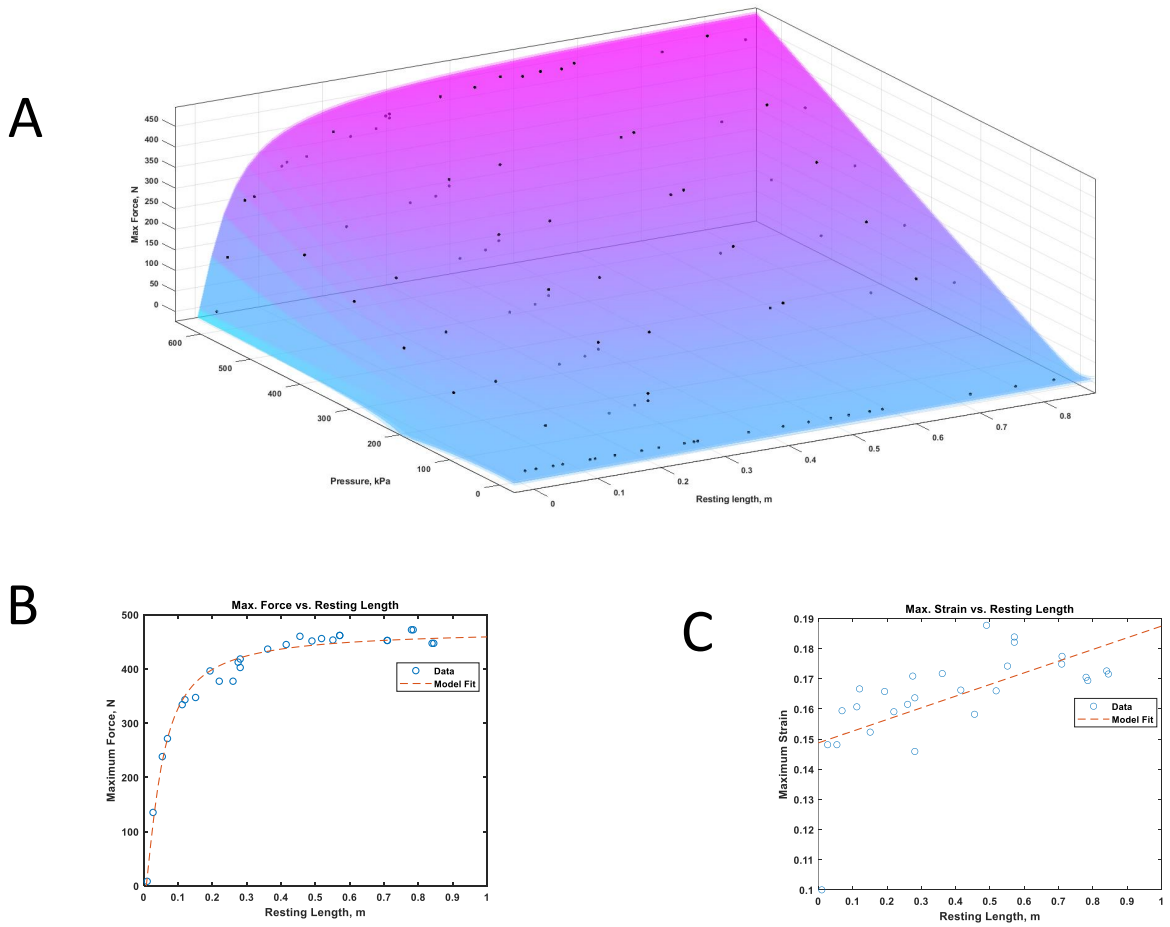

Figure 8. Results for finding the relationship between l_{rest} and $F_{max_{10}}$, ϵ_{max}. **(A)** Surface fit for $F_{max_{10}}(l_{rest}, P)$. **(B)** $F_{max_{10}}$ versus l_{rest} at $P_{max} = 620\,\text{kPa}$. **(C)** ϵ_{max} versus l_{rest} at $P_{max} = 620\,\text{kPa}$. No conclusive relationship between ϵ_{max} and l_{rest} could be deduced from this experiment.

for validation. Eq. 9 has an Adjusted $R^2 = 0.9998$, SSE $= 0.007833$, and an RMSE $= 0.0057$. Validation SSE $= 0.482595$ and RMSE $= 0.044292$. Combining Eq. 9 and Eq. 7 will now allow researchers to determine the force F in a BPA given l_{rest}, P, and ϵ^*.

$$F(\epsilon^*, P^*, l_{rest}) = F^*(\epsilon^*, P^*) \cdot F_{max}(l_{rest}) \tag{10}$$

Force functions for $\phi 20\,\text{mm}$ and $\phi 40\,\text{mm}$ BPAs were also derived. Isometric force tests were not performed on these BPA sizes. Instead, values of $F_{max_{20}} = 1500\,\text{N}$, $F_{max_{40}} = 6000\,\text{N}$, $\epsilon_{max} = 25\%$, and $P_{max} = 600\,\text{kPa}$, provided by Festo Corporation (Corporation, 2022) were used. The normalized for equation for the $\phi 20\,\text{mm}$ BPA is

$$F^*(\epsilon^*, P^*) = -0.1881 + \exp\left(-7.965 \cdot \epsilon^* - 1.677\right) + P \cdot \exp\left(-2.036 \cdot (\epsilon^{*2}\right) - 0.1518 + 0.1518 \cdot P^* \tag{11}$$

From this equation, it can be seen that the coefficient $b4 = -b5$. Eq. 11 has an Adjusted $R^2 = 0.9985$, SSE $= 0.0125$, and an RMSE $= 0.0154$. The $\phi 40\,\mathrm{mm}$ BPA fit equation is

$$F^*(\epsilon^*, P^*) = -0.06974 + \exp\left(-8.547 \cdot \epsilon^* - 2.6287\right) + P \cdot \exp\left(-0.2854 \cdot (\epsilon^*) + 1.148 - 2.128 \cdot P^*\right) \quad (12)$$

It can be seen that 12 is similar to the structure of Eqns. 8 and 11, but with an ϵ^* term in the second exponential instead of ϵ^{*2}. Eq. 12 has an Adjusted $R^2 = 0.9999$, SSE $= 8.614 \times 10^{-4}$, and an RMSE $= 0.0040$.

The new method of calculating $10\,\mathrm{mm}$ BPA force is used to calculate maximum isometric torque for the various configurations. Starting with the simplest case, we examine BPAs of $45.7\,\mathrm{cm}$ and $48.5\,\mathrm{cm}$ resting lengths on the pinned knee used for knee flexion 10. Fig. 10**A** shows measured torque as blue diamonds and expected (theoretical) torque as a magenta line. Experimentally measured values of BPA length, pressure, and moment arm were used with Eq. 10 to back calculate torque values. It was determined that a major part of the discrepancy in measured versus expected torque values was due to differences in measured versus expected ϵ^* values (Fig. 10**B**). After running an optimization algorithm to change the length of the end cap fitting, Fig. 10**C** shows improved results. The results of the optimization were validated with the $45.7\,\mathrm{cm}$ isometric torque values 10**D**. The fitting length in the algorithm is changed from $25.4\,\mathrm{mm}$ to $35.2\,\mathrm{mm}$. The optimization yielded an SSE $= 554.6$ and the validation returned a SSE $= 315.3$ with a RMSE $= 2.96$.

Pinned knee extensor results using $10\,\mathrm{mm}$ ID Festo BPAs of $41.5\,\mathrm{cm}$, $45.7\,\mathrm{cm}$ and $48.5\,\mathrm{cm}$ resting lengths are shown in Fig. 11. Measured torque was slightly higher than expected in the $48\,\mathrm{cm}$ BPA whereas it was slightly lower than expected in the $45.7\,\mathrm{cm}$ BPA. The $41.5\,\mathrm{cm}$ BPA was used in two configurations: with and without an artificial tendon. Previous optimization wasn't used with these results.

Why the discrepancy between the results? The first two seem acceptable, but not perfect. The shorter the resting length, the more the results are less than expected. Comparing measured values of l_m and ϵ^* to theoretical shows a close correlation, but would increase torque for the first two and decrease for the second. The BPA w/ artifical tendon shows a discrepancy, so maybe the tendon length was measured incorrectly? Well, maybe looking at Fig. again can shed some insight? It would be possible to bring it into the Matlab image acquisition toolbox to analyze lengths. If I can also show somehow that the shorter lengths tend to kink then that would also let us create a nonlinear torque correction factor along the lines of $M_{\hat{k}} = r\vec{k} \times (F - cf \cdot F \cdot \theta_k)$. Improved solid model might also help?

Fig. 12 shows the results optimized flexor calculation method in the biomimetic knee for a $10\,\mathrm{mm}$ ID $l_{rest} = 41.5cm$ BPA with a $12\,\mathrm{mm}$ artificial tendon made out of Shimano bicycle brake cable. Comparing the previous method of calculating torque to the measured torque results in an SSE $= 287.3$ and an RMSE $= 5.36$. The optimized torque calculation fits much better with a SSE $= 1.282$ and a RMSE $= 0.358$. Experimentally measured values were again used to back calculate torque, although we note that moment arm $r_{\hat{k}}$ was measured from knee ICR, not p_k, and that experimentally measuring $r_{\hat{k}}$ is less precise ($\pm 5\,\mathrm{mm}$) in the biomimetic knee versus the pinned knee.

Using the biomimetic knee with a $\phi 10\,\mathrm{mm}$ BPA in the extensor configuration, we obtained results for isometric torque in **??**.

Opensim comparison. Full size BPAs in biomimetic knee assembly results.

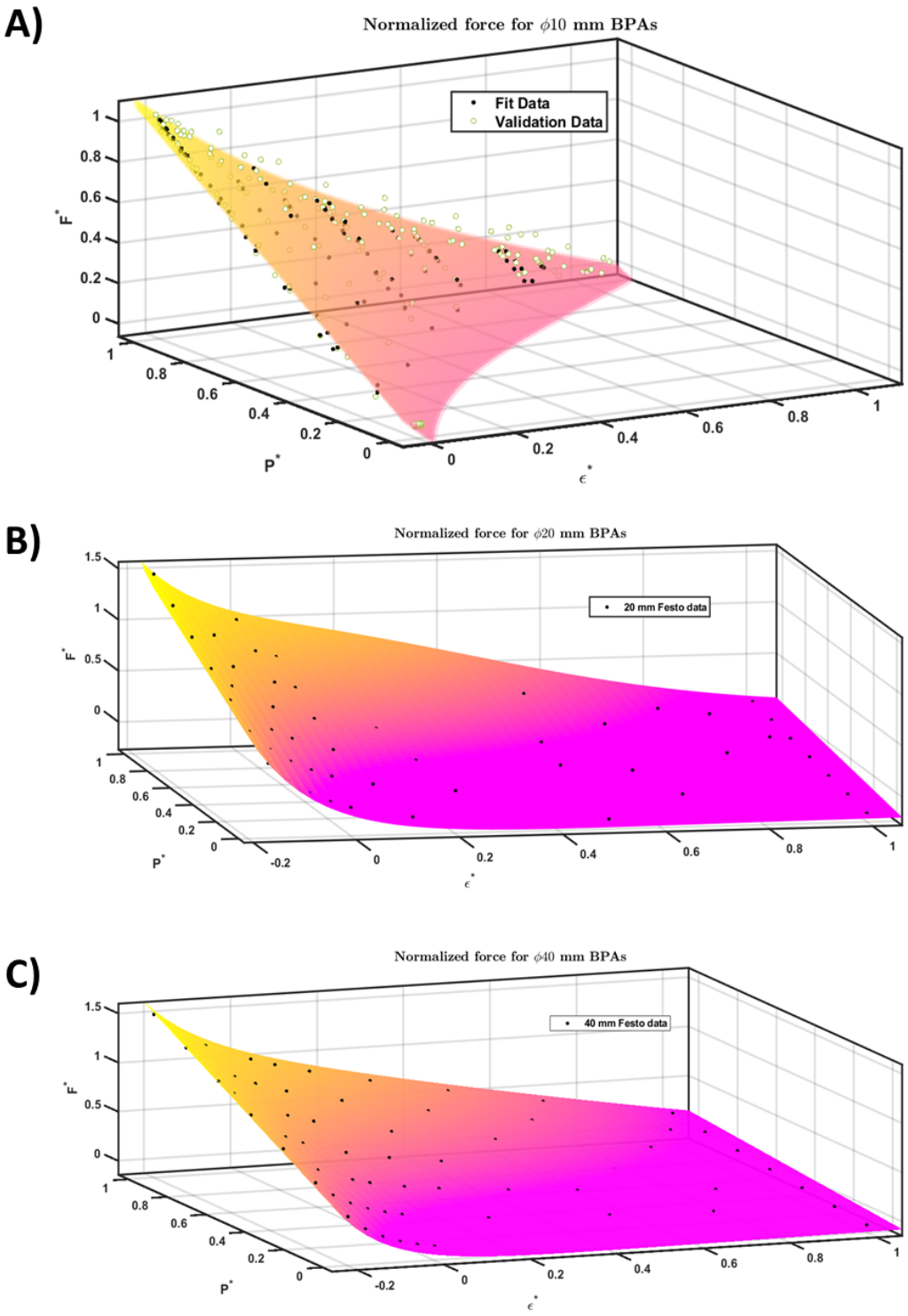

Figure 9. Surface fit for $F^*(\epsilon^*, P^*)$ with (95% CI shown). Black circles represent fit data. **(A)**Fit data for $\phi 10\,\mathrm{mm}$ Festo BPA. Validation data is the green circles. **(B)**Fit data for $\phi 20\,\mathrm{mm}$ Festo BPAs. **(C)**Fit data for $\phi 40\,\mathrm{mm}$ Festo BPAs.

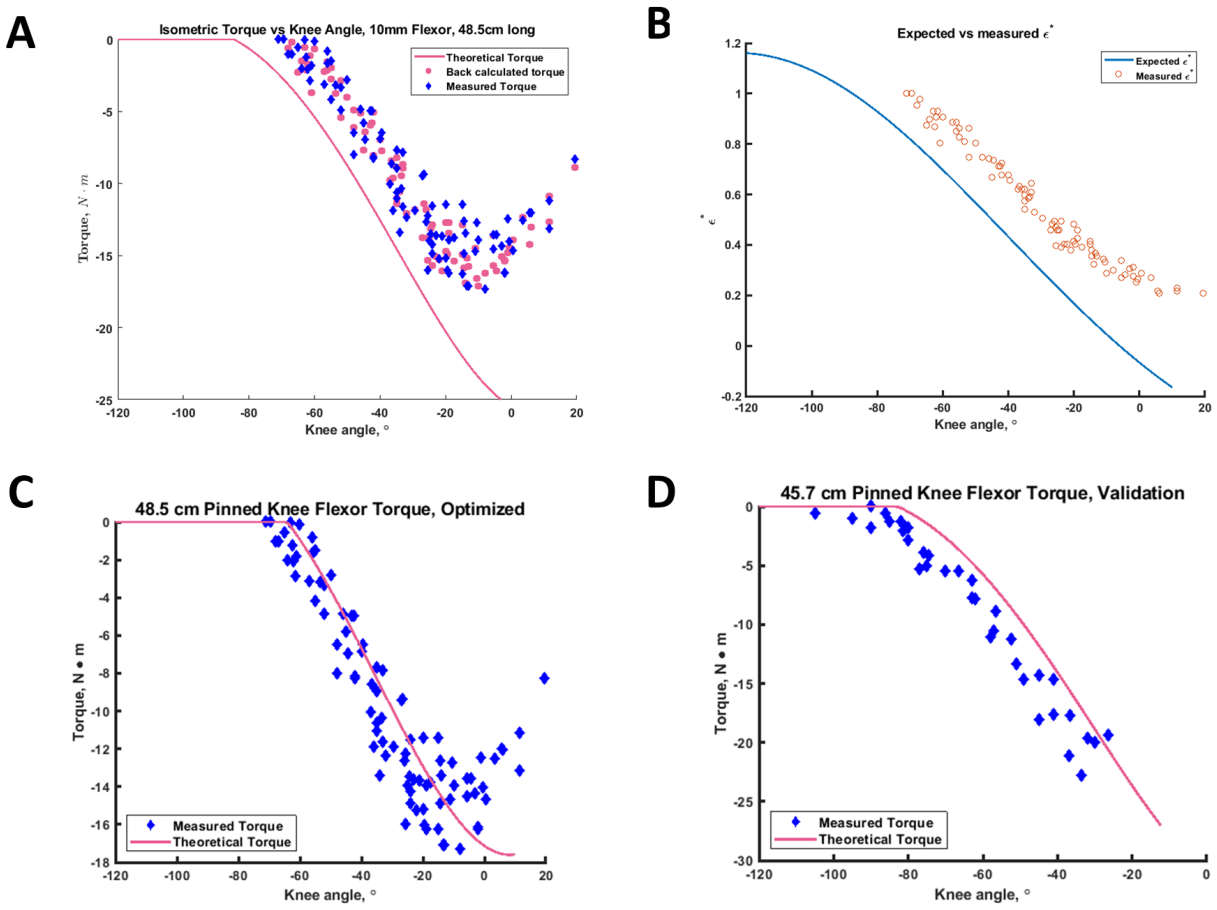

Figure 10. Results for the pinned knee using flexor BPAs. **(A)** Theoretical, measured, and back calculated torque for the $48.5\,\mathrm{cm}$ BPA. **(B)** comparison of measured versus expected ϵ^* for the $48.5\,\mathrm{cm}$ BPA. **(C)** Theoretical and measured torque for the $48.5\,\mathrm{cm}$ BPA using an optimized fitting length of $35.2\,\mathrm{mm}$. **(D)** Theoretical and measured torque for the $45.7\,\mathrm{cm}$ BPA using an optimized fitting length of $35.2\,\mathrm{mm}$

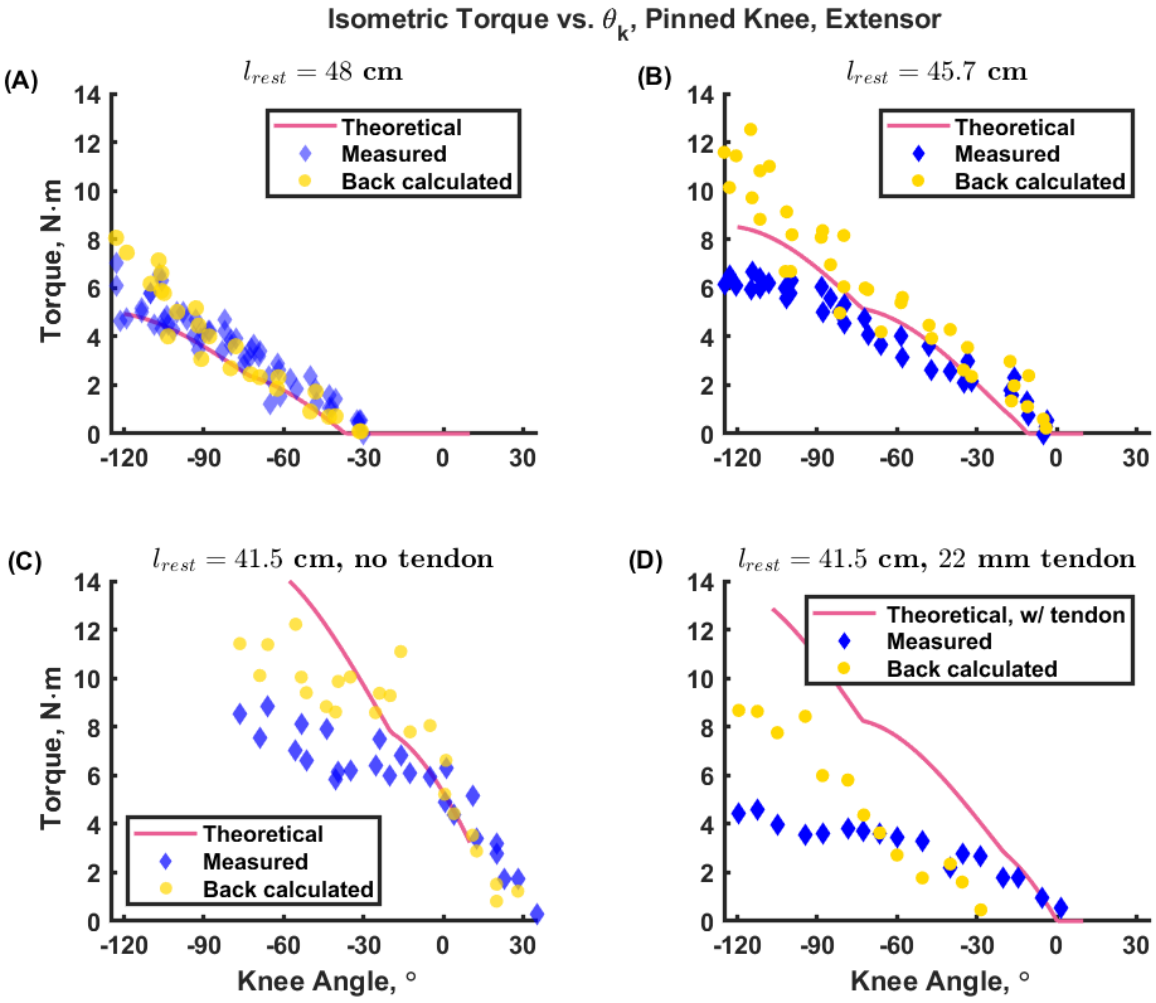

Figure 11. Pinned knee isometric torque with the extensor BPA for lengths, **(a)** 48.5 cm, **(A)** 45.5 cm, **(c)** 41.5 cm, and **(D)** 41.5 cm with a 22 mm tendon

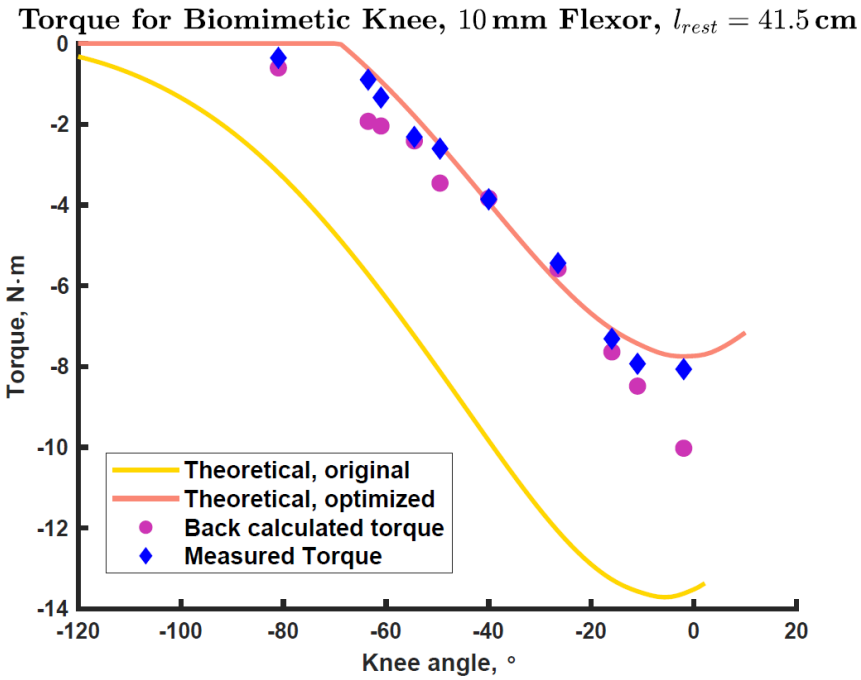

Figure 12. Biomimetic knee isometric torque for a 10 mm ID $l_{rest} = 41.5cm$ flexor BPA with a 12 mm artificial tendon. Blue diamond shows the measured torque values. Light orange line shows the theoretical torque expected using the updated actuator force equation and the optimized fitting length. The yellow line shows the theoretical torque expected using without the optimized fitting length. Magenta circles are torque values back calculated from experimentally measured values of l_m, P, and $r_{\hat{k}}$ (using measurements from knee ICR not p_k).

Figure 13. Measured versus expected isometric torque results using a ϕ10 mm, $l_{rest} = 51.8$ cm extensor BPA on the biomimetic knee.

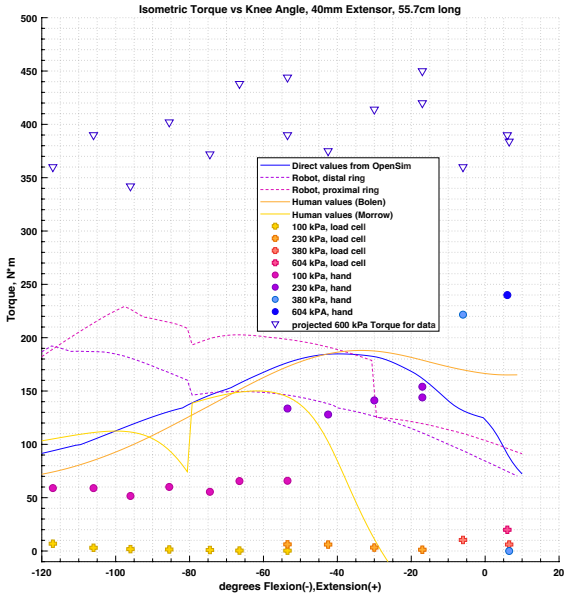

Figure 14. Comparison of isometric torque for theoretical BPA values with the humanoid knee, human muscle calculations using our method, and human muscle values as provided by OpenSim. Configurations listed are for **(A)** flexor and **(B)** extensor muscles. Note the major discrepancies between the our human value and OpenSim's, which calls into question the accuracy of our calculations.

4 DISCUSSION

The analysis in this study has allowed us to create novel equations for calculating force in BPAs of $10\,\mathrm{mm}$(Eqs. 7,9) ID.

There certainly are many factors that affect the isometric torque results.

Simplifying the model and testing it allowed us to see how we were deficient in our previous analysis. The isometric system is not rigid. It adds springiness, not

Curving BPA during high angles of knee flexion show the BPA being stretched and compressed. It is known that the axial stress in a pressure vessel is

$$\sigma_{\hat{z}} = \frac{F}{A} = \frac{Pd^2}{(d+2t)^2 - d^2} \tag{13}$$

Where $\sigma_{\hat{z}}$ is the axial stress, F is Force, A is area, P is the internal pressure, t is the wall thickness, and d is the mean diameter ($O.D. - t$). In thin wall pressure vessels 13 can be reduced to

$$\sigma_{\hat{z}} = \frac{Pd}{4t} \tag{14}$$

RESOURCE IDENTIFICATION INITIATIVE

CONFLICT OF INTEREST STATEMENT

The authors declare that the research was conducted in the absence of any commercial or financial relationships that could be construed as a potential conflict of interest.

AUTHOR CONTRIBUTIONS

BB, CM, and AH contributed to conception and design of the study. BB and CM wrote the code to calculate theoretical human and robot isometric torques. Figures were created by BB and AV. BB, LB, and AV wrote code for data collection and analysis. BB collected the data and performed the statistical analysis. BB organized the database. BB wrote the first draft of the manuscript. BB, LB, and AH wrote sections of the manuscript. All authors contributed to manuscript revision, read, and approved the submitted version.

FUNDING

Research for this article was funded by the Department of Mechanical and Materials Engineering at Portland State University, the National Science Foundation (NSF) grant for NeuroNex: Communication, Coordination, and Control in Systems (C3NS) 2015317 and NSF grant 1943483.

ACKNOWLEDGMENTS

The authors would like to acknowledge the contribution of Alex Steele, who designed the initial biomimetic 4-bar knee linkage we used for the test. He gave us solid models, built a 3D prototype, and let us break said prototype. His prompt and thoughtful responses to our questions about the previous design was very much appreciated. The authors would also like to thank Jasmine Bradley for her help reworking the figures in the results section. As a visual designer, her contributions improved the aesthetic quality of the images. She also helped us choose colors that ensured data accessibility for people with color blindness.

SUPPLEMENTAL DATA

Supplemental Data includes figures for the test setup.

DATA AVAILABILITY STATEMENT

The data sets are available from the authors upon request.

REFERENCES

Asano, Y., Okada, K., and Inaba, M. (2019). enMusculoskeletal design, control, and application of human mimetic humanoid Kenshiro. *Bioinspiration & Biomimetics* 14, 036011. doi:10.1088/1748-3190/ab03fc

Bolen, B. P. and Hunt, A. J. (2019). enDetermination of Artificial Muscle Placement for Biomimetic Humanoid Robot Legs. In *Biomimetic and Biohybrid Systems*, eds. U. Martinez-Hernandez, V. Vouloutsi, A. Mura, M. Mangan, M. Asada, T. J. Prescott, and P. F. Verschure (Cham: Springer International Publishing), vol. 11556. 15–26. doi:10.1007/978-3-030-24741-6_2

[Dataset] Corporation, F. (2022). Festo Fluidic Muscle DMSP

Delp, S., Loan, J., Hoy, M., Zajac, F., Topp, E., and Rosen, J. (1990). enAn interactive graphics-based model of the lower extremity to study orthopaedic surgical procedures. *IEEE Transactions on Biomedical Engineering* 37, 757–767. doi:10.1109/10.102791

Hoy, M., Zajac, F., and Gordon, M. (1990). A musculoskeletal model of the human lower extremity: the effect of muscle, tendon, and moment arm on the moment-angle relationship of musculotendon actuators at the hip, knee, and ankle. *Journal of Biomechanics* 23, 157–169

Hunt, A., Graber-Tilton, A., and Quinn, R. (2017). Modeling length effects of braided pneumatic actuators. In *IDETC/CIE 2017* (Cleveland, OH: ASME)

Millard, M., Uchida, T., Seth, A., and Delp, S. L. (2013). enFlexing Computational Muscle: Modeling and Simulation of Musculotendon Dynamics. *Journal of Biomechanical Engineering* 135, 021005. doi:10.1115/1.4023390

Morrow, C., Bolen, B., and Hunt, A. (2020). enOptimization of Artificial Muscle Placements for a Humanoid Bipedal Robot. In *Biomimetic and Biohybrid Systems*

Seth, A., Hicks, J. L., Uchida, T. K., Habib, A., Dembia, C. L., Dunne, J. J., et al. (2018). enOpenSim: Simulating musculoskeletal dynamics and neuromuscular control to study human and animal movement. *PLOS Computational Biology* 14, e1006223. doi:10.1371/journal.pcbi.1006223

[Dataset] Seth, A., Sherman, M., Reinbolt, J. A., and Delp, S. L. (2011). OpenSim: a musculoskeletal modeling and simulation framework for in silico investigations and exchange.

Sherman, M. A., Seth, A., and Delp, S. L. (2013). enWhat is a Moment Arm? Calculating Muscle Effectiveness in Biomechanical Models Using Generalized Coordinates. In *Volume 7B: 9th International Conference on Multibody Systems, Nonlinear Dynamics, and Control* (Portland, Oregon, USA: American Society of Mechanical Engineers), V07BT10A052. doi:10.1115/DETC2013-13633

Shin, H., Ikemoto, S., and Hosoda, K. (2018). Constructive understanding and reproduction of functions of gluteus medius by using a musculoskeletal walking robot. *Advanced Robotics* 32, 202–214. doi:10.1080/01691864.2018.1434015. Publisher: Taylor & Francis

Steele, A., Hunt, A., and Etoundi, A. (2018). Biomimetic Knee Design to Improve Joint Torque and Life for Bipedal Robotics (Bristol, UK)

Steele, A. G., Hunt, A., and Etoundi, A. C. (2017). enDevelopment of a Bio-inspired Knee Joint Mechanism for a Bipedal Robot. In *Biomimetic and Biohybrid Systems* (Springer, Cham), Lecture Notes in Computer Science, 418–427. doi:10.1007/978-3-319-63537-8_35

Thelen, D. G. (2003). enAdjustment of Muscle Mechanics Model Parameters to Simulate Dynamic Contractions in Older Adults. *Journal of Biomechanical Engineering* 125, 70–77. doi:10.1115/1.1531112

Yamaguchi, G. T. and Zajac, F. E. (1989). enA planar model of the knee joint to characterize the knee extensor mechanism. *Journal of Biomechanics* 22, 1–10. doi:10.1016/0021-9290(89)90179-6

Young, F., Rode, C., Hunt, A., and Quinn, R. (2019). enAnalyzing Moment Arm Profiles in a Full-Muscle Rat Hindlimb Model. *Biomimetics* 4, 10. doi:10.3390/biomimetics4010010

FIGURES

TABLES

Table 1. Muscle origin and insertion locations for different models. Origin is in femur reference frame, insertion is in the tibia reference frame.

Muscle	Origin/Insertion	Model	X (m)	Y (m)	Z (m)
Flexor	origin	Pinned knee	-0.075	0.100	0.0328
Flexor	insertion	Pinned knee	-0.05011	-0.045	0.0326
Extensor	origin	Pinned knee	0.030	-0.050	0
Extensor	insertion	Pinned knee	0.0425	-0.076	0
Bifemsh	origin	Gait2392	0.005	-0.211	0.023
Bifemsh	insertion	Gait2392	-0.03	-0.036	0.029
Vastus int.	origin	Gait2392	0.029	-0.192	0.031
Vastus int.	insertion	Gait2392	moving	moving	0.0018
Flexor, $10\,\mathrm{mm}$	origin	Biomimetic knee	-0.050	-0.045	0.0328
Flexor, $10\,\mathrm{mm}$	insertion	Biomimetic knee	-0.0279	-0.046	0.0328
Extensor, $10\,\mathrm{mm}$	origin	Biomimetic knee	0.040	0.035	0
Extensor, $10\,\mathrm{mm}$	insertion	Biomimetic knee	0.021	-0.072	0
Flexor, $40\,\mathrm{mm}$	origin	Biomimetic knee	-0.050	-0.045	0.0328
Flexor, $40\,\mathrm{mm}$	insertion	Biomimetic knee	-0.0279	-0.046	0.0328
Extensor, $40\,\mathrm{mm}$	origin	Biomimetic knee	0.040	0.035	0
Extensor, $40\,\mathrm{mm}$	insertion	Biomimetic knee	0.022	-0.072	0